ACS APPLIED MATERIALS & INTERFACES

Research Article

www.acsami.org

Selective Hydrothermal Method To Create Patterned and Photoelectrochemically Effective Pt/WO_3 Interfaces

Michel G. C. Zoontjes, Mark Huijben, Jonas Baltrusaitis, Wilfred G. van der Wiel, and Guido Mul*

MESA+ Institute for Nanotechnology, University of Twente, P.O. Box 217, 7500 AE Enschede, The Netherlands.

ABSTRACT: A hydrothermal method based on the use of hydrogen peroxide is described to grow a homogeneous layer of tungsten oxide (WO_3) on a platinum (Pt) film supported on a silicon wafer. WO_3 growth is highly selective for Pt when present on silicon in a patterned arrangement, demonstrating that Pt catalyzes decomposition of the WO_3 precursor in solution. The obtained Pt/WO_3 interface yields high photocurrents of 1.1 mA/cm^2 in photoelectrochemical water splitting when illuminated by a solar simulator. The photocurrents are significantly higher than most previously reported values for hydrothermally grown layers on indium−tin oxide and fluorine−tin oxide glasses. The selective growth method thus provides new options to effectively implement WO_3 in photoelectrochemical devices.

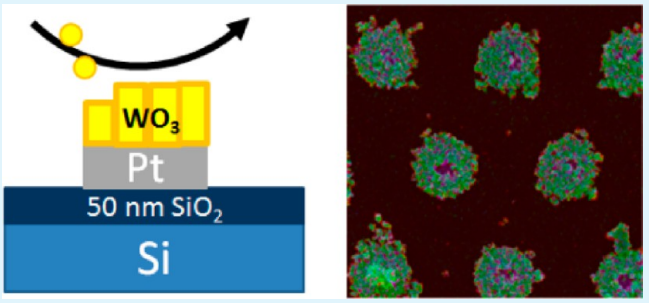

KEYWORDS: *tungsten oxide, platinum, hydrothermal synthesis, patterning, photocatalysis*

INTRODUCTION

Tungsten oxide (WO_3) is one of the most frequently studied binary oxides in photoelectrochemical cells, functioning as a photoanode.[1] Furthermore, photocatalytic application of WO_3 ranges from water purification (dye degradation) to visible-light-induced splitting of water into hydrogen and oxygen. In the latter application, WO_3 shows high water oxidation efficiency in the presence of other specific semiconducting oxides, such as modified $SrTiO_3$, thus creating a so-called Z-scheme configuration.[2] Particles and supported layers of WO_3 can be grown in various morphologies and crystal composition by several synthesis methods.[3−7] In particular, hydrothermal growth has led to compositions effective in the above-mentioned applications.[8,9] A method employing hydrogen peroxide (H_2O_2) has recently been demonstrated to yield WO_3 particles with well-defined morphologies, without the need for structure-directing additives.[10,11] When a seed layer was used, homogeneous WO_3 layers were successfully grown on indium−tin oxide (ITO)-coated glass substrates.[12,13]

Growth of WO_3 on metal surfaces has not been extensively studied, while having control over the growth of well-defined WO_3 layers on (patterned) metal surfaces is highly relevant for the creation of new device concepts in photoelectrochemistry. We hypothesize a favorable electron transfer from photoexcited WO_3 to a metal, and in particular platinum (Pt), based on the frequently reported positive effect of Pt nanoparticles on the photocatalytic performance of WO_3. This is typically assigned to electron scavenging by the Pt nanoparticles, enhancing the lifetime of excited states.[14,15] Furthermore, Nozik et al. propose the use of inequality of work functions to create an electron flow from the semiconductor to metal,[16] on which basis a photoelectrochemical diode was constructed and shown to be effective in water splitting.[17]

The objective of this study is to demonstrate the controlled growth of WO_3 on a silicon (Si)-supported Pt thin film. We modified the hydrothermal process described by others,[12,13] to obtain well-defined WO_3 layers without the need of a seeding layer. We confirm a catalytic effect of Pt in the formation of the WO_3 layers by demonstrating the growth to be selective on Pt when present on Si in a patterned arrangement. Finally, we demonstrate excellent efficiency of the Pt/WO_3 composition in photoelectrochemical applications.

EXPERIMENTAL SECTION

A 100-nm-thick Pt film was sputtered on an oxidized ⟨100⟩ Si wafer. To allow strong adhesion, a 13 nm titanium (Ti) layer was used between the substrate and film. Sputtering was performed using in-house-developed sputtering equipment, applying a 6.6 mbar argon atmosphere. For Pt and Ti, 2 in. targets were used and a 200 W direct-current sputter was applied.

A dot pattern was defined in the Ti/Pt film using photolithography and passive ion beam etching with Ar^+ ions in an Oxford Ionfab 300 reactive ion beam etching system.

WO_3 layers were grown hydrothermally on the Pt surface, without the need of a seeding layer. H_2WO_4 (Sigma Aldrich) was dissolved in 35% H_2O_2 (Sigma Aldrich) to a concentration of 0.5 M at 80 °C under vigorous stirring. After cooling to room temperature, this solution was diluted to 0.01 M H_2WO_4 by the addition of distilled water. Two slightly different procedures for growth were followed. In the first procedure, 20 mL of the 0.01 M solution was transferred directly after into a Teflon beaker and inserted in a stainless steel autoclave [a 4748

Received: September 12, 2013
Accepted: November 20, 2013
Published: November 20, 2013

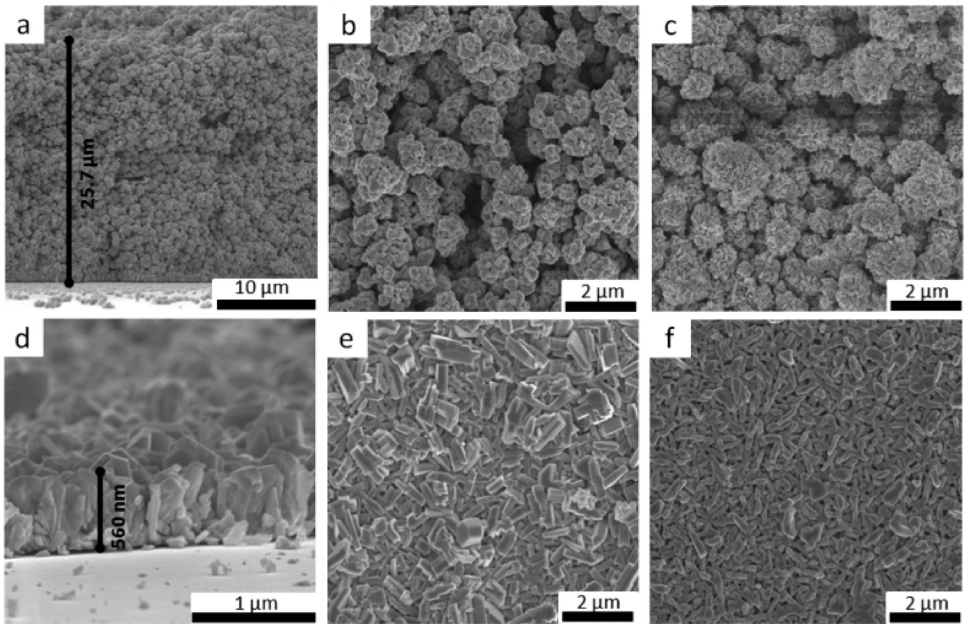

Figure 1. SEM images of hydrothermally grown WO_3 layers: (a and b) side and top views of flower-type layers formed in the presence of excess H_2O_2; (c) top view of the layer after subsequent annealing at 600 °C; (d and e) side and top views of an as-prepared rod-type layer in lower concentrations of H_2O_2, induced by decomposition of excess H_2O_2 prior to hydrothermal treatment; (f) top view of the layer after subsequent annealing at 600 °C.

acid digestion vessel (Parr Instruments)]. This was followed by immersion of the $Si/SiO_2/Ti/Pt$ substrate, closure of the autoclave, and hydrothermal treatment at 170 °C for 18 h, applying a heating rate of 10 °C/min. In the second procedure, the 0.01 M solution was pretreated overnight at room temperature by two small pieces of the $Si/SiO_2/Ti/Pt$ substrate with a total area of approximately 1 cm^2. Oxygen evolution due to decomposition of the excess of H_2O_2 was initially clearly visible. The gas evolution stopped after overnight treatment. The pieces were removed, and synthesis was continued in hydrothermal conditions as described for the first procedure by adding the solution and $Si/SiO_2/Ti/Pt$ substrate to the Teflon beaker. For both procedures, after the digestion vessel was cooled to room temperature by a natural cool down, the substrates were removed from the solution, carefully rinsed with distilled water, and dried under a mild nitrogen flow. Finally, the samples were annealed at 600 °C for 12 h in static air, applying a heating rate of 10 °C.

Characterization of the grown layers was performed by high-resolution scanning electron microscopy (HR-SEM) and X-ray diffraction (XRD) analysis. For imaging, a Nova 600-nanolab HR-SEM instrument (FEI Instruments) was used, and for combined imaging/elemental mapping, a Merlin HR-SEM (Metrology Zeiss) system, equipped with an energy-dispersive X-ray spectroscopy (EDX) instrument, was used. A Bruker D2 powder diffractometer (equipped with a Cu Kα source) was used for analysis of the WO_3 crystal structure.

Electrochemical measurements were performed in a three-electrode cell setup equipped with a Versastat 4 potentiostat (Princeton). A 1.5AM solar simulator (model 10500, ABET Technologies) was applied as the light source. The reactor consisted of a 25 mL optical glass cuvette, which filtered most of the emitted UV light. The counter electrode (EC) consisted of a Pt mesh connected to a Pt wire. A 3.0 M Ag/AgCl reference electrode (BASi) was used, with a potential of +0.210 V vs. NHE. This value can be converted to V_{RHE} by the Nernst equation:

$$V_{RHE} = V_{Ag/AgCl} + V_{Ag/AgCl\ vs\ RHE} + 0.059pH \quad (1)$$

Contact to the Si-supported Pt/WO_3 working electrode was accomplished by a stainless steel clamp, protected from the electrolyte by encapsulation in an epoxy resin. The WO_3 layer was faced toward the light source. The electrolyte consisted of a 0.3M H_3PO_4 solution.

RESULTS AND DISCUSSION

The morphology of the WO_3 layers hydrothermally grown on Pt in the presence of H_2O_2 can be composed of two different morphologies; see Figure 1. WO_3 grown in the presence of an excess of H_2O_2 shows a flower-like morphology (Figure1a,b) and a high porosity. Cross-sectional views indicate a thickness of this porous layer of around 25 μm. When the excess of H_2O_2 in the precursor solution was allowed to decompose prior to hydrothermal WO_3 growth, a dense layer with crystals in a rod-like morphology is obtained (Figure 1d,e). Side-view measurements show a thickness of 560 nm. This thickness is rather independent of the time of hydrothermal treatment because a large fraction of WO_3 crystallizes in solution. After annealing at 600 °C (Figure 1c,f), the layers hardly change their morphology; only some facets appear to become more rounded.

Besides the large differences in the thickness and morphology, a large difference in adhesion of the WO_3 layer to the Pt film was observed for the two different hydrothermal procedures. The rod-shaped crystals showed strong adhesion upon rinsing and drying procedures, while the thick and porous flower-like layers were substantially washed off when exposed to the same procedure. These characterization results demonstrate the large effect of the absence or presence of an excess of H_2O_2 on the surface morphology. Although we did not investigate this aspect, Jiao et al.[12] attributed the morphology differences to the absence or presence of a WO_3 seeding layer on their applied fluorine-doped tin oxide (FTO)-coated glass. With a (spin-coated) WO_3 seeding layer, a rod-like morphology was obtained, whereas without the seeding layer, WO_3 crystals with high porosity and flower-like shape were formed.

XRD was applied to characterize the crystal phase of the grown layers; see Figure 2. The diffraction lines of Pt and Si of the substrates are visible at 40.0 and 47.4°. The WO_3 crystals of both layer morphologies consist of $WO_3 \cdot 0.33H_2O$ (JCPDS 87-

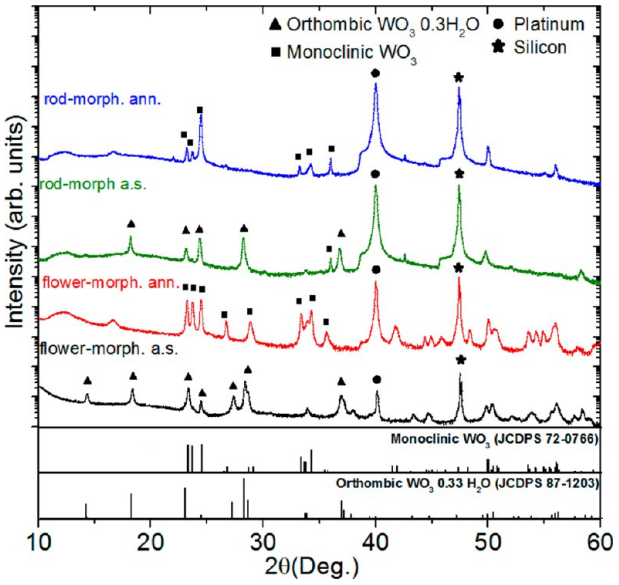

Figure 2. XRD patterns of the WO_3 layers with rod- and flower-type morphologies before and after annealing at 600 °C. As synthesized, both morphologies exhibit a tungsten oxide hydrate phase. By annealing, this hydrate phase is converted to the monoclinic tungsten oxide phase.

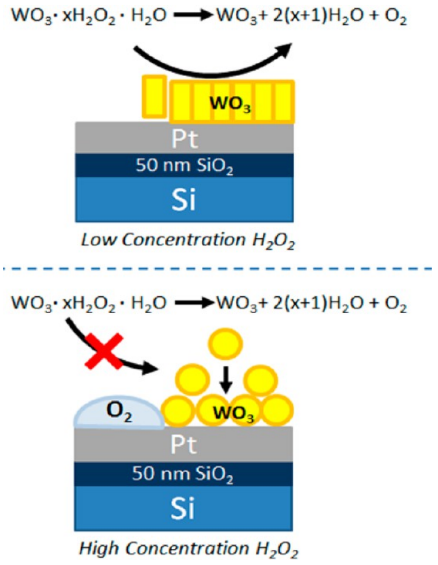

Figure 3. Schematic overview of the two proposed growth mechanisms for WO_3 at Pt surfaces in the presence of low and high concentrations of H_2O_2, respectively. In the presence of high concentrations of H_2O_2, oxygen bubbles are formed, resulting in a porous (flower-type) WO_3 layer loosely attached to the Pt layer. For low concentrations of H_2O_2, peroxopolytungstic acid decomposes on the Pt surface, and a strongly adhering WO_3 layer is formed.

1203), with the main diffraction lines at 14.3 and 18.2°, as well as two additional characteristic lines around 23.4 and 24.2°. After annealing at 600 °C, the monoclinic WO_3 phase is formed (JCDPS 72-0766) with three main characteristic diffraction lines at 23.2, 23.7, and 24.4°, which are representative of the [200], [020], and [002] crystal planes, respectively. In the case of the rod-like morphology, there seems to be a preferential orientation in the [002] direction of the crystal, while in the case of the flower-like morphology, the distribution for the [200], [020], and [002] planes is approximately equal.

The following two reactions are proposed to describe the process of WO_3 formation:[12]

$$H_2WO_4 + xH_2O_2 \xrightarrow{\text{heating}} WO_3 \cdot xH_2O_2 \cdot H_2O \quad (2)$$

$$WO_3 \cdot xH_2O_2 \cdot H_2O \xrightarrow{\text{Pt surface}} WO_3(\text{layer}) + 2(x+1)H_2O + O_2(g) \quad (3)$$

Following eq 2, the tungstic acid and H_2O_2 are converted to a WO_3 precursor containing peroxide and water (peroxopolytungstic acid). The peroxide-containing complex is subsequently converted to (supported) WO_3 crystals and oxygen (eq 3), presumably catalyzed by the Pt surface. The differences in adhesion, crystal orientation, and morphology of WO_3 on Pt relate to the applied H_2O_2 concentration in the precursor solution. In high concentrations of H_2O_2, Pt catalyzes decomposition of H_2O_2, which is in competition with decomposition of the peroxopolytungstic acid intermediate. H_2O_2 decomposition leads to extensive formation of O_2 bubbles, inhibiting decomposition of peroxopolytungstic acid at the Pt substrate. Presumably, WO_3 crystals grow extensively in solution and subsequently deposit on the substrate, which affects WO_3 adhesion and yields the obtained highly porous morphology. A schematic overview of the two proposed mechanisms for growth is provided in Figure 3.

To evaluate the proposed catalytic effect of Pt in peroxopolytungstic acid decomposition, preferential growth of WO_3 on Pt was attempted, as was previously reported for ZnO nanostructures on gold nanoparticles.[18−20] To this end, a Pt pattern of 10 and 50 μm sized dots was prepared on a Si/SiO_2/Ti substrate by microlithography. After application of the hydrothermal growth procedure with a relatively low concentration of H_2O_2, the formation of WO_3 was analyzed by SEM in combination with EDX. The results are shown in Figure 4. SEM images with representative EDX maps are shown for the 50 μm dots (Figure 4a,b) and the 10 μm dots (Figure 4c,d), respectively. The SEM images confirm the preferential growth of WO_3 crystals on the Pt dots. Mapping of the specific elements, i.e., Si (red), Pt (magenta), W (green), and O (blue), was performed using EDX. Between the dots, a dominant red color is visible and represents the Si substrate. On the dots, the main colors are green and blue, confirming the presence of W and O. Traces of the Pt substrate are visible in the 50 μm dots, while the EDX result suggests the formation of a less dense WO_3 layer on the 10 μm sized dots. Only a small part of the Pt film appears not to be covered by WO_3.

To analyze the properties of the interface of the Pt film and the deposited WO_3 crystals, photoelectrochemical characterization was performed, of which the results are shown in Figure 5. During the final annealing step, the thick layers with the flower-like morphology detached from the Pt surface because of low adhesion. Therefore, it was not possible to use these samples in the photoelectrochemical setup and measure the photocurrent. The cyclic voltammetry curves of the dense WO_3 layer are compared to the curves of the bare Pt layer (on the Si/SiO_2 substrate) in Figure 5a. In both cases, at an applied potential of 1.7 V versus reversible hydrogen electrode (RHE), the current is measured and assigned to electrolysis of H_2O. Oxygen is formed at the working electrode [the bare Pt substrate or the WO_3 layer (black curve in Figure 5a), respectively], while hydrogen is formed at the counter electrode

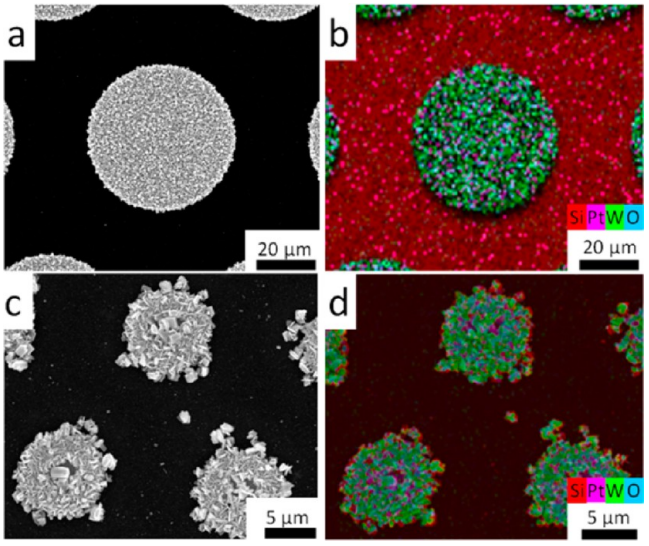

Figure 4. Images of WO_3 layers grown at patterned Pt surfaces on Si, obtained by SEM combined with elemental mapping by EDX. (a) SEM images of 50-μm-diameter Pt/WO_3 dots and (b) the corresponding EDX map of Si, Pt, W, and O. (c) SEM images of 10-μm-diameter Pt/WO_3 dots and (d) the corresponding EDX map of Si, Pt, W, and O.

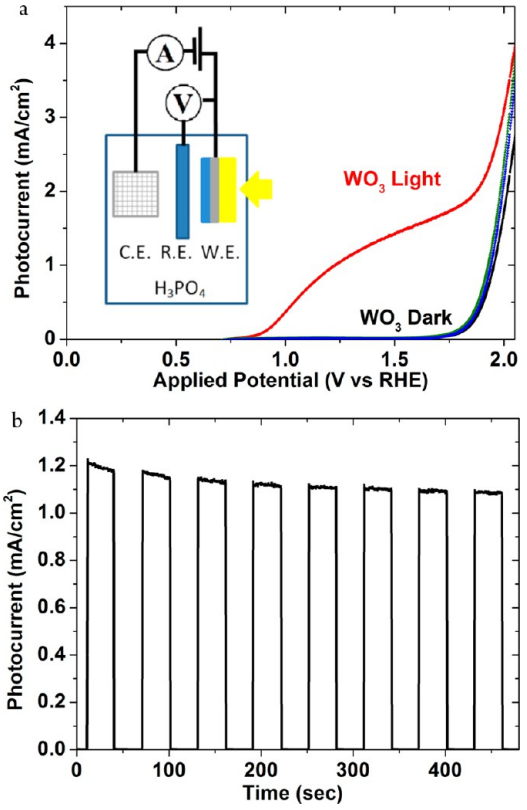

Figure 5. Photocurrent measurements of the WO_3 layer (grown in relatively low concentrations of H_2O_2) in a 0.3M H_3PO_4 electrolyte. A scan rate of 50 mV/s was applied. (a) *I*–*V* curves of the Si/Pt substrate (dark is the blue line; light is the green line) and a Si/Pt/WO_3 sample (dark is the black line; light is the red line). Clearly, the photocurrent is measured for the WO_3 layer, when exposed to light. The inset shows the measurement configuration used for the measurements. (b) Chronoamperometry measurement of the WO_3 layer. The applied bias was 1.23 V vs RHE. A clear change in the photocurrent between light on and off is measured.

(a Pt mesh). This is confirmed by the electrochemical water-splitting potential of 1.73 V typically obtained with two Pt electrodes, being the result of a theoretical value of 1.23 V, and a 0.5 V overpotential for water oxidation. When a 1.5 AM solar simulator is used to illuminate the substrates, the bare Pt film does not show a photoresponse, as expected. On the other hand, for the WO_3 layer, a clear photoresponse is measured. The onset potential where oxygen evolution is initiated has decreased from 1.7 to 0.75 V vs RHE, which indicates a shift of 0.95 V by illumination of WO_3. The photocurrent obtained at a bias potential of 1.23 V is about 1.1 mA/cm^2.

To further characterize the response of the system, a chronoamperometry measurement was performed; see Figure 5b. The sample was intermittently exposed to light in periods of 30 s at a bias potential of 1.23 V vs RHE. When the sample was illuminated, a photocurrent of about 1.1 mA/cm^2 was measured, in agreement with the curve of Figure 5a. The photoresponse was relatively independent of the number of light exposure cycles, demonstrating the reproducibility of the photoresponse and high stability of the WO_3 layer.

According to the Shockley–Queisser limit, the maximum achievable photocurrent at 1.5 AM solar irradiation for WO_3 (2.6 eV band gap) is 6.0 mA/cm^2.[21,22] The 1.1 mA/cm^2 value is thus 18.3% of the maximum achievable photocurrent. In the literature, a range of photocurrents are reported for supported WO_3 layers, typically obtained with different light sources. For example, a high photocurrent of 2.6 mA/cm^2 was reported for nitrogen-doped WO_3, but this was achieved with a 500 W xenon lamp emitting light of high intensity.[23] Photocurrents measured with a 1.5 AM solar simulator are included in Table 1 for comparison. The photocurrents in the table are the values at 1.23 V vs RHE. With the Nernst equation, the potentials were corrected for differences in the pH and the reference electrode used. Compared to other hydrothermally grown layers, our WO_3 layers at Pt substrates show a significantly higher photocurrent. This confirms the favorable electron transfer of photoexcited WO_3 to the Pt film and is in agreement with a high electron conductivity. The photocurrent of 1.1 mA/cm^2 is lower than the photocurrent reported by Hong et al. This might be related to the thickness of the WO_3 layer (3.3 μm, prepared by polymer-assisted deposition in the study of Hong et al., vs 0.5 μm in the present study), as well as to the high crystallinity of the layers prepared by Hong et al.[26] The onset potentials obtained with our layers showed values comparable to those reported for conductive glass substrates, so the Schottky barrier between WO_3 and Pt, if unfavorable, does not appear to significantly inhibit electron transfer.

CONCLUSION

We demonstrate that by use of a hydrothermal method growth of WO_3 in intimate contact with a Pt film can be achieved. The growth is likely controlled by the Pt-catalyzed decomposition of a peroxopolytungstic acid intermediate, as confirmed by the spatial distribution achieved using Si surfaces equipped with Pt dots. A tungsten oxide hydrate phase is thus formed, which is converted upon annealing to a monoclinic WO_3 phase. The Pt-supported layers show a significant photoresponse of 1.1 mA/cm^2 at a bias potential of 1.23 V vs RHE. This response is significantly higher than most previously reported values for hydrothermally grown layers on ITO and FTO glass. This is highly relevant for the creation of new devices for photo-

Table 1. Selected Literature Overview of Photocurrents Obtained for WO_3 Layers Using a 1.5 AM Solar Simulator

material system	growth method	electrolyte	photocurrent [mA/cm^2]	onset [V vs RHE]	reference
WO_3 at Pt	hydrothermal growth	0.3 M H_3PO_4	1.1	0.75	this work
WO_3 at SnO_2:F-coated glass	hydrothermal growth	0.5 M H_2SO_4	0.6	0.45	Hong et al.[24]
WO_3 at SnO_2:F-coated glass	hydrothermal growth	1 M H_2SO_4	0.4	0.55	Jiao et al.[13]
WO_3 at SnO_2:F-coated glass	reacting RF magnetron sputtering	0.33 M H_3PO_4	1.1	0.95	Marsen et al.[25]
WO_3 at SnO_2:F-coated glass	polymer-assisted deposition	0.5 M H_2SO_4	2.3	0.60	Hong et al.[26]
WO_3 at SnO_2:F-coated glass	chemical solution deposition	1 M $HClO_4$	2.3	0.45	Santato et al.[27]

electrochemical production of hydrogen. Future studies will involve the use of other metal films and study of the effect of the composition of such a film on formation of the WO_3 layer, as well as on the achievable photocurrents. Further, the patterned surfaces might find application in advanced sensing and photoelectrochemical devices, requiring efficient metal−semiconductor interfaces.

AUTHOR INFORMATION

Corresponding Author

*E-mail: G.Mul@utwente.nl.

Notes

The authors declare no competing financial interest.

ACKNOWLEDGMENTS

This work was supported by the Strategic Research Orientation "Nanomaterials for Energy", MESA + Institute for Nanotechnology, University of Twente, Twente, The Netherlands. W.G.v.d.W. acknowledges financial support from the European Research Council (ERC Starting Grant 240433). We acknowledge Mark Smithers and Johnny Sanderink for the SEM images and Saurabh Bose for assistance in the ion etching of Pt.

REFERENCES

(1) Zheng, H.; Ou, J. Z.; Strano, M. S.; Kaner, R. B.; Mitchell, A.; Kalantar-zadeh, K. *Adv. Funct. Mater.* **2011**, *21*, 2175−2196.

(2) Kato, H.; Hui, M.; Konta, R.; Shimodaira, Y.; Kudo, A. *Chem. Lett.* **2004**, *33*, 1348−1349.

(3) Kim, C.-Y.; Lee, M.; Huh, S.-H.; Kim, E.-K. *J. Sol−Gel Sci. Technol.* **2009**, *53*, 176−183.

(4) Li, Y. M.; Hibino, M.; Miyayania, M.; Kudo, T. *Solid State Ionics* **2000**, *134*, 171−179.

(5) Zhang, J.; Wang, X. L.; Xia, X. H.; Gu, C. D.; Tu, J. P. *Sol. Energy Mater. Sol. Cells* **2011**, *95*, 2107−2112.

(6) Santano, C.; Ulmann, M.; Augustynski, J. *Adv. Mater.* **2001**, *13*, 511−514.

(7) Lee, S. H.; Deshpande, R.; Parilla, P. A.; Jones, K. M.; To, B.; Mahan, A. H.; Dilon, A.C. *Adv. Mater.* **2006**, *18*, 763−766.

(8) Su, X.; Xiao, F.; Li, Y.; Jian, J.; Sun, Q.; Wang, J. *Mater. Lett* **2010**, *64*, 1232−1234.

(9) Hassani, H.; Marzbanzad, E.; Zamani, C.; Raissi, B. *J. Mater. Sci.: Mater. Electron.* **2011**, *22*, 1264−1268.

(10) Li, J.; Huang, J.; Yu, C.; Wu, J.; Cao, L.; Yanagisawa, K. *Chem. Lett.* **2011**, *40*, 579−581.

(11) Jiayin, L.; Jianfeng, H.; Jianpeng, W.; Liyun, C.; Yanagisawa, K. *Ceram. Int.* **2012**, *38*, 4495−4500.

(12) Jiao, Z.; Sun, X. W.; Wang, J.; Ke, L.; Demir, H. V. *J. Phys. D: Appl. Phys.* **2010**, *43*, 285501.

(13) Jiao, Z.; Wang, J.; Ke, L.; Sun, X. W.; Demir, H. V. *ACS Appl. Mater. Interfaces* **2011**, *3*, 229−236.

(14) Abe, R.; Takami, H.; Murakami, N.; Ohtani, B. *J. Am. Chem. Soc.* **2008**, *130*, 7780−7781.

(15) Xu, Z.; Tabata, I.; Hirogaki, K.; Hisada, K.; Wang, T.; Wang, S.; Hori, T. *Mater. Lett.* **2011**, 1252−1256.

(16) Halek, G.; Baikie, I. D.; Teterycz, H.; Halek, P.; Suchorska-Woźniak, P.; Wiśniewski, K. *Sens. Actuators B* **2013**, *187*, 379−385.

(17) Nozik, A. J. *Appl. Phys. Lett.* **1977**, *30*, 567−569.

(18) Fan, Z. Y.; Lu, J. G. *J. Nanosci. Nanotechnol.* **2005**, *5*, 1561−1573.

(19) Gomez, J. L.; Tigli, O. *J. Mater. Sci.* **2013**, *48*, 612−624.

(20) Greene, L. E.; Law, M.; Tan, D. H.; Montano, M.; Goldberger, J.; Somorjai, G.; Yong, P. D. *Nano Lett.* **2005**, *5*, 1231−1236.

(21) Shockley, W.; Queisser, H. J. *J. Appl. Phys.* **1961**, *32*, 510−&.

(22) Amano, F.; Li, D.; Ohtani, B. *J. Electrochem. Soc.* **2011**, *158*, K42−K46.

(23) Liu, Y.; Li, Y.; Li, W.; Han, S.; Liu, C. *Appl. Surf. Sci.* **2012**, *258*, 5038−5045.

(24) Hong, S. J.; Jun, H.; Borse, P. H.; Lee, J. S. *Int. J. Hydrogen Energy* **2009**, *34*, 3234−3242.

(25) Marsen, B.; Cole, B.; Miller, E. L. *Sol. Energy Mater. Sol. Cells* **2007**, *91*, 1954−1958.

(26) Hong, S. J.; Jun, H.; Lee, J. S. *Scr. Mater.* **2010**, *63*, 757−760.

(27) Santato, C.; Ulmann, M.; Augustynski, J. *J. Phys. Chem. B* **2001**, *105*, 936−940.